AGU PUBLICATIONS

JGR

Journal of Geophysical Research: Atmospheres

RESEARCH ARTICLE
10.1002/2015JD023890

Key Points:
- We improved two methods for adjusting T_{mean}, Pr, and their dependence in scenarios
- Methods are tested at Arctic coastal sites where T_{mean}-Pr dependence is crucial
- Both methods improve the plausibility of the local climate scenarios

Supporting Information:
- Text S1, Figures S1–S9, and Table S1

Correspondence to:
P. Grenier,
grenier.patrick@ouranos.ca

Citation:
Gennaretti, F., L. Sangelantoni, and P. Grenier (2015), Toward daily climate scenarios for Canadian Arctic coastal zones with more realistic temperature-precipitation interdependence, *J. Geophys. Res. Atmos.*, *120*, 11,862–11,877, doi:10.1002/2015JD023890.

Received 6 JUL 2015
Accepted 4 NOV 2015
Accepted article online 5 NOV 2015
Published online 1 DEC 2015

Toward daily climate scenarios for Canadian Arctic coastal zones with more realistic temperature-precipitation interdependence

Fabio Gennaretti[1,2], Lorenzo Sangelantoni[3], and Patrick Grenier[1,4]

[1]Consortium Ouranos, Montreal, Quebec, Canada, [2]Now at CEREGE, Aix-Marseille Université, Aix-en-Provence, France, [3]Department of Life and Environmental Sciences, Università Politecnica delle Marche, Ancona, Italy, [4]Centre pour l'Étude et la Simulation du Climat à l'Échelle Régionale, Université du Québec à Montréal, Montreal, Quebec, Canada

Abstract The interdependence between climatic variables should be taken into account when developing climate scenarios. For example, temperature-precipitation interdependence in the Arctic is strong and impacts on other physical characteristics, such as the extent and duration of snow cover. However, this interdependence is often misrepresented in climate simulations. Here we use two two-dimensional (2-D) methods for statistically adjusting climate model simulations to develop plausible local daily temperature (T_{mean}) and precipitation (Pr) scenarios. The first 2-D method is based on empirical quantile mapping (2Dqm) and the second on parametric copula models (2Dcopula). Both methods are improved here by forcing the preservation of the modeled long-term warming trend and by using moving windows to obtain an adjustment specific to each day of the year. These methods were applied to a representative ensemble of 13 global climate model simulations at 26 Canadian Arctic coastal sites and tested using an innovative cross-validation approach. Intervariable dependence was evaluated using correlation coefficients and empirical copula density plots. Results show that these 2-D methods, especially 2Dqm, adjust individual distributions of climatic time series as adequately as one common one-dimensional method (1Dqm) does. Furthermore, although 2Dqm outperforms the other methods in reproducing the observed temperature-precipitation interdependence over the calibration period, both 2Dqm and 2Dcopula perform similarly over the validation periods. For cases where temperature-precipitation interdependence is important (e.g., characterizing extreme events and the extent and duration of snow cover), both 2-D methods are good options for producing plausible local climate scenarios in Canadian Arctic coastal zones.

1. Introduction

Climate change impact and adaptation studies need plausible local climate scenarios covering the coming decades [*Fowler et al*., 2007; *Maraun et al*., 2010; *Maurer et al*., 2014]. When represented as time series, plausible scenarios should be characterized by the following: (1) agreement with observations in key statistical properties over relatively long comparison periods, (2) lack of discontinuities at past/future junctions, and (3) future trends simulated by state-of-the-art climate models that take into account likely evolutions of natural and anthropogenic forcing agents [*Grenier et al*., 2015]. Such scenarios are often obtained by statistically adjusting global or regional climate model simulations. The techniques employed often use transfer functions calibrated on observed and simulated climate variables over a historical period [e.g., *Chiew et al*., 2010; *Dibike and Coulibaly*, 2005; *Mpelasoka and Chiew*, 2009; *Räty et al*., 2014; *Themeßl et al*., 2012].

One important aspect of observed climates which climate scenarios should reflect is the interdependence of climatic variables. For example, temperature and precipitation are physically related through several mechanisms, such as the influence of rainfall on soil moisture, which in turn impacts on surface temperature by controlling partitioning between sensible and latent heat fluxes [*Cong and Brady*, 2012; *Huang and van den Dool*, 1993]. However, observed intervariable dependences are often misrepresented in climate model outputs, and univariate methods that adjust simulated sequences are not made to improve their realism [*Wilcke et al*., 2013]. For this reason, recent studies have investigated the possibility of applying postprocessing methods that also adjust intervariable dependences [*Ben Alaya et al*., 2014; *Hoffmann and Rath*, 2012; *Li et al*., 2014; *Piani and Haerter*, 2012; *Vrac and Friederichs*, 2014]. Some of these methods are based on parametric copula models, which are functions that describe the dependence structure between variables independently of their univariate marginal distributions [*Genest and Favre*, 2007; *Sklar*, 1959].

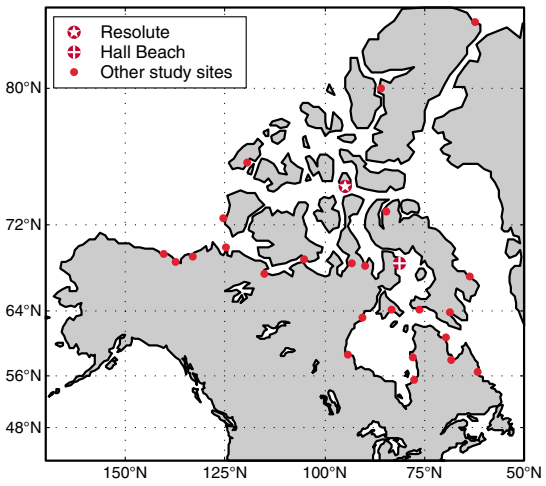

Figure 1. Study sites in the Canadian Arctic. Resolute and Hall Beach are highlighted as they are selected as examples in other figures.

Intervariable dependence is not a fixed characteristic but varies spatially and seasonally [*Cong and Brady*, 2012]. For example, the temperature-precipitation interdependence in Canada tends to increase with latitude and is particularly strong in the Arctic regions [*Isaac and Stuart*, 1992], where it impacts other fundamental physical characteristics, such as the extent and duration of snow cover [*R. D. Brown*, 2000; *Vaughan et al.*, 2013; *Ye and Cohen*, 2013]. There are several reasons to build local Arctic climate scenarios with more realistic intervariable dependence. First, such scenarios would potentially allow for a better characterization of future extreme events [*S. J. Brown et al.*, 2014]. Second, meteorological intervariable consistency is essential for determining the future extent and duration of snow cover and sea ice [*R. D. Brown*, 2000; *Germe et al.*, 2014; *Vaughan et al.*, 2013; *Ye and Cohen*, 2013], as well as for improving modeling of streamflow (especially during snowmelt), permafrost thaw, and lake water level [*Carroll et al.*, 2011; *Smith et al.*, 2005; *Thorne*, 2011].

In this paper, we compare temperature-precipitation interdependence in observations and model outputs at 26 Canadian Arctic coastal sites and improve two recently published two-dimensional (2-D) statistical adjustment methods to produce climate scenarios. More specifically, we use the gridded interpolated Canadian database of daily minimum and maximum temperatures and precipitation for 1950–2010 [*McKenney et al.*, 2011] as a benchmark to assess interdependence realism in a representative ensemble of 13 model simulations from the Coupled Model Intercomparison Project Phase 5 (CMIP5). Subsequently, we investigate how the modeled temperature-precipitation dependence structures at the study sites are modified by both a common one-dimensional (1Dqm) and the two proposed 2-D postprocessing techniques. One 2-D method (2Dqm) is based on empirical quantile mapping as suggested by *Piani and Haerter* [2012] and the other (2Dcopula) on the use of parametric copula models as suggested by *Li et al.* [2014]. Both methods are improved by two modifications suggested by univariate statistical adjustment studies. First, we adjust the data for each day of the year differently in order to respect seasonal variations of the climate variables [*Themeßl et al.*, 2012; *Thrasher et al.*, 2012]. Second, we handle temperature values to force the preservation of the modeled warming trend [*Hempel et al.*, 2013; *Wood et al.*, 2004]. Results show the realism of the temperature-precipitation interdependence in the scenarios' time series for a variety of sites, simulations, postprocessing techniques, and times of the year over the calibration/validation period 1981–2010. An innovative approach for performing cross validation is also presented.

2. Materials and Methods

2.1. Study Sites and Observational Data

We selected for this study 26 Canadian Arctic coastal sites that have daily weather station records of both temperature and precipitation. Site locations are shown in Figure 1, whereas toponyms and coordinates are listed in Table 1. To avoid discontinuities in the time series, the nearest grid node to each station of the Natural Resources Canada 10×10 km interpolated data set (hereafter referred to as NRCan; http://cfs.nrcan.gc.ca/projects/3/4; [*McKenney et al.*, 2011]) is used as the observational product rather than station records. The NRCan data set contains daily minimum and maximum temperatures (T_{min} and T_{max}) as well as daily precipitation (Pr). We obtained the mean daily temperature using the approximation $T_{mean} = (T_{min} + T_{max})/2$ for each site. The study period is 1981–2010.

Table 1. Study Sites[a]

No.	Site	Latitude	Longitude	Kind of Site[b]	Canadian Province or Territory
1	Kuujjuarapik	55.3	−77.8	Community	Quebec
2	Nain	56.5	−61.7	Community	Newfoundland and Labrador
3	Kuujjuaq	58.1	−68.4	Community	Quebec
4	Inukjuak	58.5	−78.1	Community	Quebec
5	Churchill	58.7	−94.1	Community	Manitoba
6	Quaqtaq	61.0	−69.6	Community	Quebec
7	Chesterfield Inlet	63.3	−90.7	Community	Nunavut
8	Iqaluit	63.8	−68.6	Community	Nunavut
9	Cape Dorset	64.2	−76.5	Community	Nunavut
10	Coral Harbour	64.2	−83.4	Community	Nunavut
11	Fox-5, Broughton Island	67.5	−63.8	Radar Station, site of the DEW Line	Nunavut
12	Kugluktuk	67.8	−115.2	Community	Nunavut
13	Kugaaruk	68.5	−89.8	Community	Nunavut
14	Hall Beach	68.8	−81.3	Community, site of the DEW Line	Nunavut
15	Shepherd Bay	68.8	−93.4	Radar Station, site of the DEW Line	Nunavut
16	Shingle Point	68.9	−137.2	Radar Station, site of the DEW Line	Yukon
17	Cambridge Bay	69.1	−105.1	Community, site of the DEW Line	Nunavut
18	Tuktoyaktuk	69.4	−133.0	Community, site of the DEW Line	Northwest Territories
19	Komakuk Beach	69.6	−140.2	Radar Station, site of the DEW Line	Yukon
20	Cape Parry	70.2	−124.7	Radar Station, site of the DEW Line	Northwest Territories
21	Sachs Harbour	72.0	−125.3	Community	Northwest Territories
22	Nanisivik	73.0	−84.6	Dismissed mining company town	Nunavut
23	Resolute	74.7	−95.0	Community	Nunavut
24	Mould Bay	76.2	−119.3	Weather station	Northwest Territories
25	Eureka	80.0	−85.9	Research station	Nunavut
26	Alert	82.5	−62.3	Military and scientific base	Nunavut

[a]Sites are ordered from the southernmost (top) to the northernmost (bottom).
[b]DEW Line means distant early warning line, a system of radar stations established during the Cold War.

2.2. Model Data

Methods are assessed using 13 global climate model simulations. Initially, we considered 30 simulations with ensemble member r1i1p1 from CMIP5 historical/RCP4.5 experiments (see Tables 2 and S1 in the supporting information). Daily values of T_{mean} and *Pr* over the 1981–2010 period were interpolated to the study sites. Next, to reduce redundancy, a smaller but representative ensemble was selected based on a cluster analysis [*Logan et al*., 2011; *Houle et al*., 2012]. For that we created a matrix in which we stacked the mean and standard deviation of the climatic variables (daily T_{mean} and *Pr*) for each site and each simulation (30 rows × 120 columns matrix, where 30 is the number of simulations initially considered and 120 results from 30 sites × 2 variables × 2 statistical properties). The matrix values were then normalized independently for each column, and a series of *k*-means clustering analyses were conducted by iteratively increasing the number of clusters (starting from one) and retaining only the simulations nearest to one cluster centroid at each iteration. The smallest subset explaining at least 80% of the original ensemble's variance was finally selected for the subsequent analyses; this amounted to 13 simulations (Table 2).

2.3. Postprocessing Methods

In total, four alternative methods for obtaining climate scenarios are used in this study: (1) using simulations directly as scenarios (hereafter DirectSim scenarios), (2) a 1-D method based on quantile mapping (1Dqm), (3) a 2-D method based on quantile mapping, and (4) a 2-D method based on copula models. Other 2-D

Table 2. Models Used in This Study[a]

Modeling Center[b]	Model	Selected by Cluster Analysis
BCC	BCC-CSM1.1	
BCC	BCC-CSM1.1(m)	
CCCma	CanCM4	x
CCCma	CanESM2	
CMCC	CMCC-CM	x
CMCC	CMCC-CMS	
CNRM-CERFACS	CNRM-CM5	x
CSIRO-BOM	ACCESS1.0	
CSIRO-BOM	ACCESS1.3	
CSIRO-QCCCE	CSIRO-Mk3.6.0	x
GCESS-BNU	BNU-ESM	x
INM	INM-CM4	x
IPSL	IPSL-CM5A-LR	
IPSL	IPSL-CM5A-MR	
IPSL	IPSL-CM5B-LR	x
LASG-CESS	FGOALS-g2	x
MIROC	MIROC-ESM	x
MIROC	MIROC-ESM-CHEM	
MIROC	MIROC4h	x
MIROC	MIROC5	
MOHC	HadCM3	
MOHC	HadGEM2-CC	
MOHC-INPE	HadGEM2-ES	x
MPI-M	MPI-ESM-LR	x
MPI-M	MPI-ESM-MR	
MRI	MRI-CGCM3	
NCC	NorESM1-M	x
NOAA-GFDL	GFDL-CM3	
NOAA-GFDL	GFDL-ESM2G	
NOAA-GFDL	GFDL-ESM2M	

[a]For each of the 30 models, the simulation of the experiment historical/RCP4.5 with ensemble member r1i1p1 was considered, but in the end only 13 simulations were selected by cluster analysis for the subsequent analyses.
[b]Full names for the modeling centers are provided in Table S1.

methods that restrict the duration of scenarios to that of the observational product and that cannot be easily adapted to respect the long-term simulated trend are not considered [e.g., *Vrac and Friederichs*, 2014].

The 1Dqm method adjusts daily T_{mean} and *Pr* separately and is based on the empirical quantile mapping technique [*Déqué*, 2007; *Themeßl et al.*, 2012]. The basic idea of quantile mapping is to first describe the mismatch between simulated and observed distributions at specific quantiles and then to apply a transfer function, defined as the operation that must be performed on each quantile of the simulated distribution to obtain the corresponding observed quantile. For example, if the simulated and observed T_{mean} distributions have their 25th percentile at 13°C and 16°C, respectively, then the transfer function has a +3°C value for 13°C. The transfer function is next used to adjust each simulated value, even those out of the calibration period. In our case, the transfer function $F(x)$ is computed at 51 fixed percentile values [$\mathrm{Sim}P_i$ where $i = \{0, 2, 4, \ldots, 100\}$], and $F(x \neq \mathrm{Sim}P_i)$ is linearly interpolated if $\mathrm{Sim}P_0 < x < \mathrm{Sim}P_{100}$ or held constant beyond these boundary values [$F(x < \mathrm{Sim}P_0) = F(\mathrm{Sim}P_0)$ and $F(x > \mathrm{Sim}P_{100}) = F(\mathrm{Sim}P_{100})$]. Modifications to this basic procedure are often applied (see, for example, section 2.4).

Like 1Dqm, the 2Dqm method uses the basic quantile mapping idea, but some changes are made to more realistically reproduce the temperature-precipitation interdependence. Here we first adjust dry day frequencies in the simulated time series, as done by *Schmidli et al.* [2006] (see the *Pr* adjustment of the 2Dcopula below). T_{mean} values for wet and dry days are then corrected with two separate quantile mappings. Finally, *Pr* for wet days is adjusted following the steps suggested by *Piani and Haerter* [2012]: (1) In both the observed and simulated values, the daily *Pr* and T_{mean} data pairs over the calibration period are ordered according to T_{mean} ranks, and equally sized subsets are defined (here eight subsets: up to the 12.5th percentile, between the 12.5th and 25th percentiles, and so on). (2) Within each subset, an independent quantile mapping is performed on the *Pr* values. (3) The adjusted *Pr* daily values are sorted back to their original Julian day. Simulated *Pr* values are thus adjusted differently according to the T_{mean} of their corresponding day. A schematic diagram illustrating the 2Dqm procedure is provided in Figure 2, and Figure S1 illustrates how *Pr* may differ between each subset at one site.

The 2Dcopula adjustment is based on parametric copula models which, following Sklar's theorem [1959], allow the dependence structure of a joint cumulative distribution function (joint CDF: $H(x, y)$) to be described as follows:

$$H(x,y) = C\{F(x), G(y)\}, \quad x, y \in R \tag{1}$$

where $F(x)$ and $G(y)$ are the marginal CDF of two variables, and C is the copula CDF. Copula and marginals are independent from one another. Here we model the observed and simulated *Pr* and T_{mean} marginal

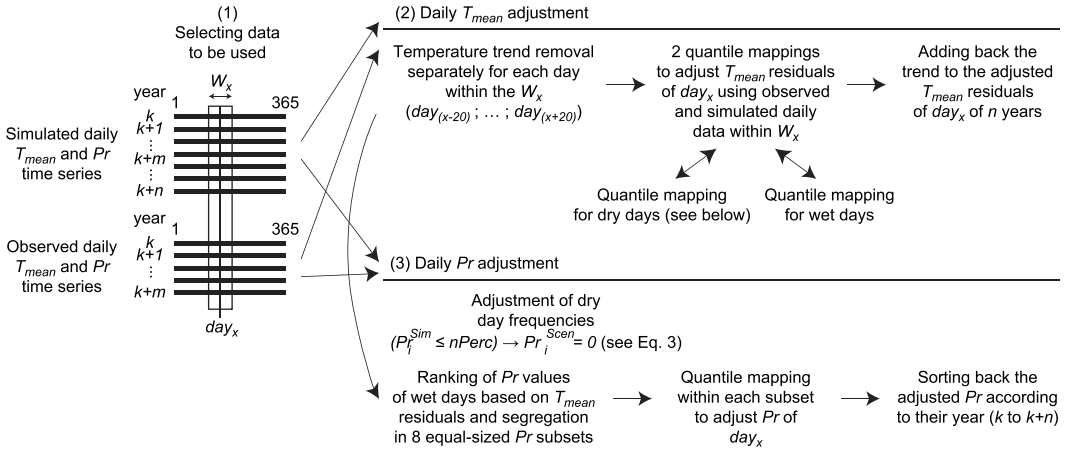

Figure 2. Diagram illustrating the 2Dqm adjustment of the data for 1 day of the year (day_x where x can vary from 1 to 365) at one site for one simulation. The transfer functions in steps (2) and (3) are based on quantile mappings calibrated to years k to $k+m$ to adjust simulated data of years k to $k+n$.

distributions and their joint behavior using gamma (for *Pr* marginal distribution), Gaussian (for T_{mean} marginal distribution), and Gaussian copula (for the dependence structure) functions for each site and simulation over the calibration period. Once these functions' parameters are determined, the adjustment of simulated daily *Pr* and T_{mean} proceeds by adjusting first T_{mean}, and next *Pr* conditional upon the probability associated to T_{mean}, as explained by *Li et al*. [2014]. However, unlike the original method and similarly to our 2Dqm, we define the joint intervariable behavior (i.e., copula functions) on wet days only, after the previous adjustment of dry/wet day frequencies. This expedient also allows T_{mean} to be modeled for wet and dry days with different Gaussian functions, thus improving the scenario results (not shown). The steps of the 2Dcopula adjustment for simulated T_{mean} and *Pr* values at day *i* are described in further detail below.

Step 1: T_{mean} *adjustment*.

$$\begin{cases} \left(Pr_i^{\text{Sim}} \le n\text{Perc}\right) \rightarrow T_{\text{mean}_i}{}^{\text{Scen}} = F1^{\text{Obs}\,-1}\left(F1^{\text{Sim}}\left(T_{\text{mean}_i}{}^{\text{Sim}}\right)\right) \\ \left(Pr_i^{\text{Sim}} > n\text{Perc}\right) \rightarrow T_{\text{mean}_i}{}^{\text{Scen}} = F2^{\text{Obs}\,-1}\left(F2^{\text{Sim}}\left(T_{\text{mean}_i}{}^{\text{Sim}}\right)\right) \end{cases} \tag{2}$$

Step 2: *Pr adjustment*.

$$\begin{cases} \left(Pr_i^{\text{Sim}} \le n\text{Perc}\right) \rightarrow Pr_i^{\text{Scen}} = 0 \\ \left(Pr_i^{\text{Sim}} > n\text{Perc}\right) \rightarrow p = C^{\text{Sim}}\left\{F2^{\text{Sim}}\left(T_{\text{mean}_i}{}^{\text{Sim}}\right), G^{\text{Sim}}\left(Pr_i^{\text{Sim}}\right)\right\} \\ \qquad\qquad Pr_i^{\text{Scen}} = G^{\text{Obs}\,-1}\left(C^{\text{Obs}\,-1}\left\{F2^{\text{Obs}}(\ldots), G^{\text{Obs}}(\ldots)\right|\left(F2^{\text{Obs}}(\ldots) = F2^{\text{Sim}}\left(T_{\text{mean}_i}{}^{\text{Sim}}\right), C^{\text{Obs}}(\ldots) = p\right)\right\}\right) \end{cases} \tag{3}$$

where Sim and Obs refer to simulation and observations over the calibration period, Scen refers to scenarios over the study period, F_1 and F_2 are the T_{mean} marginal CDFs for dry and wet days, G is the *Pr* marginal CDF for wet days, C is the copula CDF, and *n*Perc is the *n*th percentile of the simulated precipitation values over the calibration period, *n* indicating the percentage of dry days in the observations.

2.4. Method Modifications

For all adjustment methods (1Dqm, 2Dqm, and 2Dcopula), we also employ the following two modifications proposed by univariate adjustment studies to improve the scenarios. First, we use moving windows (41 days centered on the day of the year to be adjusted, considering all years within the calibration period) to determine the transfer functions between simulated and observed climate values used in the adjustment procedure [*Themeßl et al*., 2012; *Thrasher et al*., 2012]. Moving windows allow for an adjustment that varies smoothly from one day of the year to another. Second, temporal trends in temperature (i.e., linear trends calculated separately for simulated and observed time series and for each day of the year) are removed prior to statistical adjustment in order to obtain a stationary adjustment procedure (i.e., one not influenced by the

trend-induced inflation of the variability [*Scherrer et al*., 2005]). Trends are subsequently added back to the T_{mean} time series. This modification is similar to what *Hempel et al*. [2013] and *Wood et al*. [2004] proposed and guarantees the preservation of the long-term trend from the simulation to the scenario; this property can otherwise be altered by the statistical adjustments. Figure 2 illustrates how moving windows and temperature time trend preservation are integrated in the 2Dqm procedure, whereas in section 3.3 we show the impact of these modifications on the 2Dqm method.

2.5. Cross-Validation Scheme

A cross-validation scheme is applied to assess the methods' performance. For that, we calibrate over three different 20 year periods within 1981–2010 and assess the scenarios' plausibility over the remaining 10 year blocks (1981–1990, 1991–2000, or 2001–2010). Cross validation has previously been used in climatological studies [e.g., *Lafon et al*., 2013; *Li et al*., 2010; *Stoner et al*., 2013; *Thrasher et al*., 2012], with the objective of validating whether scenario-generating methods can predict a block of data not used in the calibration [*Maraun et al*., 2015]. Here we work with an alternative cross-validation approach that does not compare the validation data with each individual scenario, but rather with the ensemble of scenarios as a whole. This approach is consistent with interpreting each individual scenario not as a prediction but as a plausible climate trajectory among many alternatives [*Mearns et al*., 2001] that may diverge from one another due to nonsynchronized internal variability [*Fischer et al*., 2014]. However, if individual scenarios are equiprobable and form a reliable predictive ensemble, then a large number of independent validation cases (each with its own ensemble of scenarios) should result in the validation data occupying all possible ranks within the ensembles of scenarios equally often. A relevant statistical tool for this exercise is the verification rank histogram [*Wilks*, 2011], previously used in climatological studies [e.g., *Oldenborgh et al*., 2013; *Grenier et al*., 2015]. The sharpness of the results of the ensembles of scenarios is also verified using boxplots. By sharpness, we mean here a reduced spread of the scenario ensemble members around the observational statistics.

3. Results

3.1. Adjustment of the Marginal Distributions

As a first step, each generated scenario has been visually evaluated with quantile-quantile plots (e.g., Figure 3). This shows that all methods (1Dqm and 2-D) adjust marginal distributions quite well. For T_{mean}, quantile-quantile values for adjusted scenarios are close to the diagonals, meaning the distributions of the daily data are similar in observations and scenarios. Conversely, DirectSim scenarios are characterized by larger, temperature-dependent offsets, specific to each site and model. For example, Figure 3a shows a DirectSim scenario with an almost constant positive offset that shifts around 0°C, probably because the model misrepresents physical processes associated with the freezing point. This is a common characteristic among the simulations and has also been observed in studies of other regions [e.g., *Casati et al*., 2013]. For *Pr*, 1Dqm could have been expected to perform better than 2-D methods because the adjustment is not conditioned by the T_{mean} values. However, visual evaluation reveals that the 1Dqm and 2-D methods produce similar improvements relative to DirectSim scenarios, even if the quantile-quantile values are generally farther from the diagonals than in the case of T_{mean}, especially for extreme values (e.g., Figure 3b). This is because precipitation extremes are highly variable and the transfer functions' fit is worse. It is worth mentioning that our methods, based on moving windows (41 days centered on the day to be adjusted), are implemented not to exactly reproduce the observational sequences but to develop scenarios that are intended to be interpreted as plausible climate trajectories.

The plausibility of the T_{mean} and *Pr* marginal distributions in the scenarios has subsequently been analyzed with the cross-validation scheme using Kolmogorov-Smirnov tests and two custom metrics (termed m_{center} and $m_{extremes}$ metrics; see supporting information). The Kolmogorov-Smirnov test allows for testing the null hypothesis that observed and scenario data are drawn from the same parent distribution (Figures 4 and S2), while the two custom metrics are implemented to specifically quantify dissimilarities in the central part of the univariate distributions (m_{center} metric; Figures S3 and S4) and in the extreme values ($m_{extremes}$ metric; Figures S5 and S6). Annual daily values are examined, as well as daily values of a winter month (January) and a summer month (July).

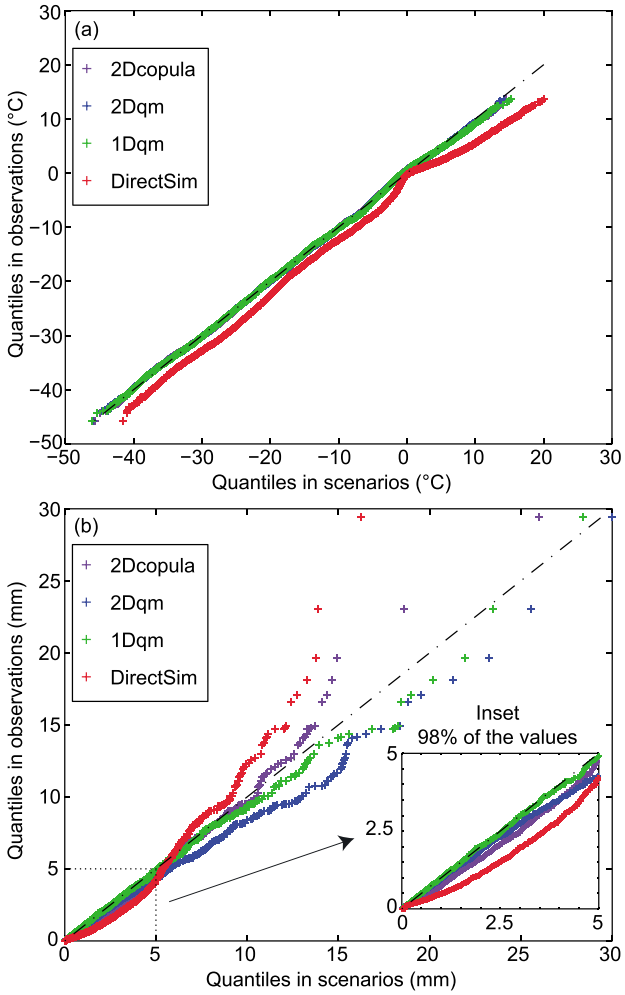

Figure 3. Quantile-quantile plots of observed versus scenario annual daily climatic data (1981–2010 period using value of the three 10 year validation blocks) showing the results of the adjustment methods for one model (MIROC-ESM) at one site (Resolute) selected as examples. (a) Temperature (note that the results for 2Dcopula, 1Dqm, and 2Dqm are almost coincident and their plus symbols cannot be differentiated). (b) Precipitation.

These goodness-of-fit tests generalize the results of the visual evaluation and allow us to conclude that all adjustment methods (1Dqm, 2Dqm, and 2Dcopula) lead to significant improvements in the marginal distributions relative to DirectSim scenarios, and that the 2-D methods are as good as 1Dqm. In the case of T_{mean}, all adjustments result in similar positive cross-validation statistics (Figures S2, S4, and S6). In the case of *Pr*, scenarios based on quantile mapping (1Dqm and 2Dqm) agree better with the observations than 2Dcopula scenarios do over the calibration period (Figures 4a–4c, S3, and S5). However, 1Dqm, 2Dqm, and 2Dcopula obtain similar results over the validation periods, all of them improving the sharpness of the ensembles of scenarios (Figures 4d–4f and S3) as well as the equiprobability of the observational ranks among the scenario members (Figure S3g), except for extreme values (Figures S5d–S5g). The Kolmogorov-Smirnov statistic also indicates that the higher the site's latitude, the more dissimilar the distributions of the observed and DirectSim scenario data (for both T_{mean} or *Pr*; see Figures 4 and S2). Finally, Figure S3 shows that, in general, low *Pr* values in DirectSim scenarios have positive offsets relative to observations. This is likely due to a combination of the model drizzle problem [see *Dai*, 2006] and/or underestimations of trace events in the NRCan data set [see *Mekis*, 2005].

3.2. Interdependence Between T_{mean} and *Pr*

Once the goodness-of-fit tests were completed, the interdependence between T_{mean} and *Pr* at each site was evaluated and compared among observations, DirectSim, 1Dqm, and 2-D scenarios. First, we analyzed the correlation between daily T_{mean} and *Pr*, in terms of both Spearman (Figures 5 and 6) and Pearson (Figure S7) correlation coefficients. As expected, results indicate that temperature-precipitation interdependence varies with the period of the year and the site location, as reported by other studies [*Cong and Brady*, 2012]. In January, the observational correlation coefficients are always highly significant and positive, whereas in July coefficients are generally negative or not significant depending on whether or not dry days were included (Figures 5b, 5c, 6b, 6c, S7b, and S7c). The intervariable correlation coefficients obtained with the 2-D methods are much more similar to those observed over the full calibration period for almost all site/scenario pairs and all analyzed periods of the year (Figures 5a–5c). Conversely, the DirectSim and 1Dqm scenarios are in some cases characterized by large offsets relative to the observations. DirectSim and 1Dqm also obtain similar results for both January and July data (Figures 5b, 5c, 6b, and 6c). This supports

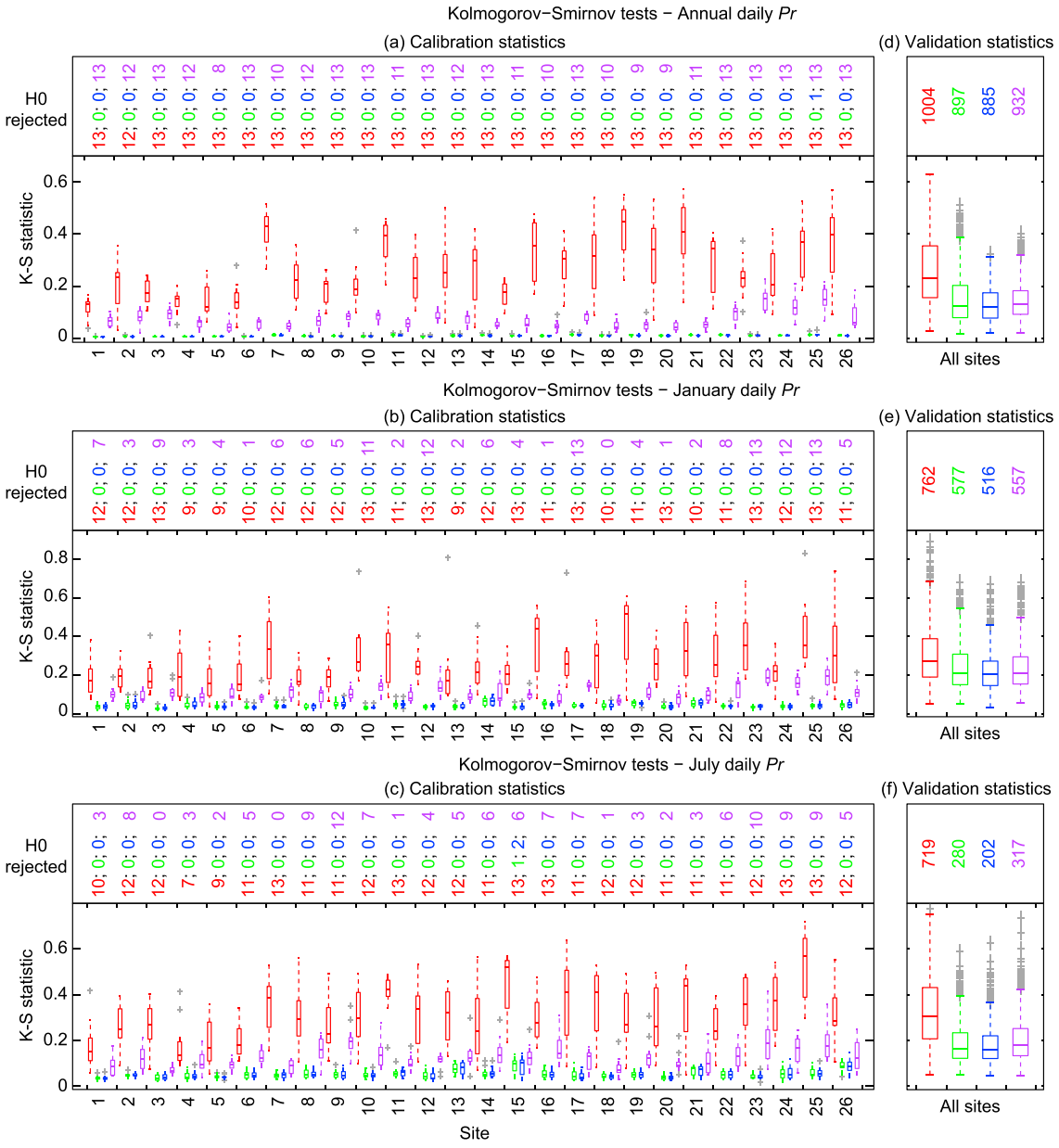

Figure 4. Kolmogorov-Smirnov statistic between observed and scenario (a and d) annual, (b and e) January, (c and f) July daily *Pr* over the full calibration period (Figures 4a–4c), and the three validation periods (Figures 4d–4f). In each pair of observed and scenario data, the *n* lower values were removed, where *n* is the maximum of the number of dry days in the observations or the scenario. The number of scenarios for which the test rejected the null hypothesis that the observed and scenario values are drawn from the same parent distribution is also indicated ($p < 0.001$). Different colors indicate values for observed versus DirectSim (red), 1Dqm (green), 2Dqm (blue), and 2Dcopula (violet) scenario data. Sites (see Table 1) are ordered from the southernmost (left) to the northernmost (right). Each box refers to 13 values (one per simulation) in Figures 4a–4c and to 1014 values (three periods × 26 sites × 13 simulations) in Figures 4d–4f. For each box, quartiles (central bar and box edges), extreme values within 1.5 interquartile ranges from the box edges (whiskers), and outliers (plus signs) are represented. The other boxplots in this paper have a similar setup.

Wilcke et al.'s [2013] previous finding that univariate adjustments do not impact modeled temperature-precipitation correlations much if the scenario's sequence (i.e., succession of low and high values) is based on the simulated one. When considering annual daily data instead, the 1Dqm method reduces the correlation offsets of the DirectSim scenarios (Figures 5a and 6a). Indeed, all proposed adjustment methods use moving windows so that summer days are subjected to different transfer functions than winter days. Thus, the annual cycle is rectified by both the 1Dqm and the 2-D methods. However, the 2-D methods also adjust the day-to-day covariation between T_{mean} and *Pr*. For this reason, over the three validation periods, the 2-D methods

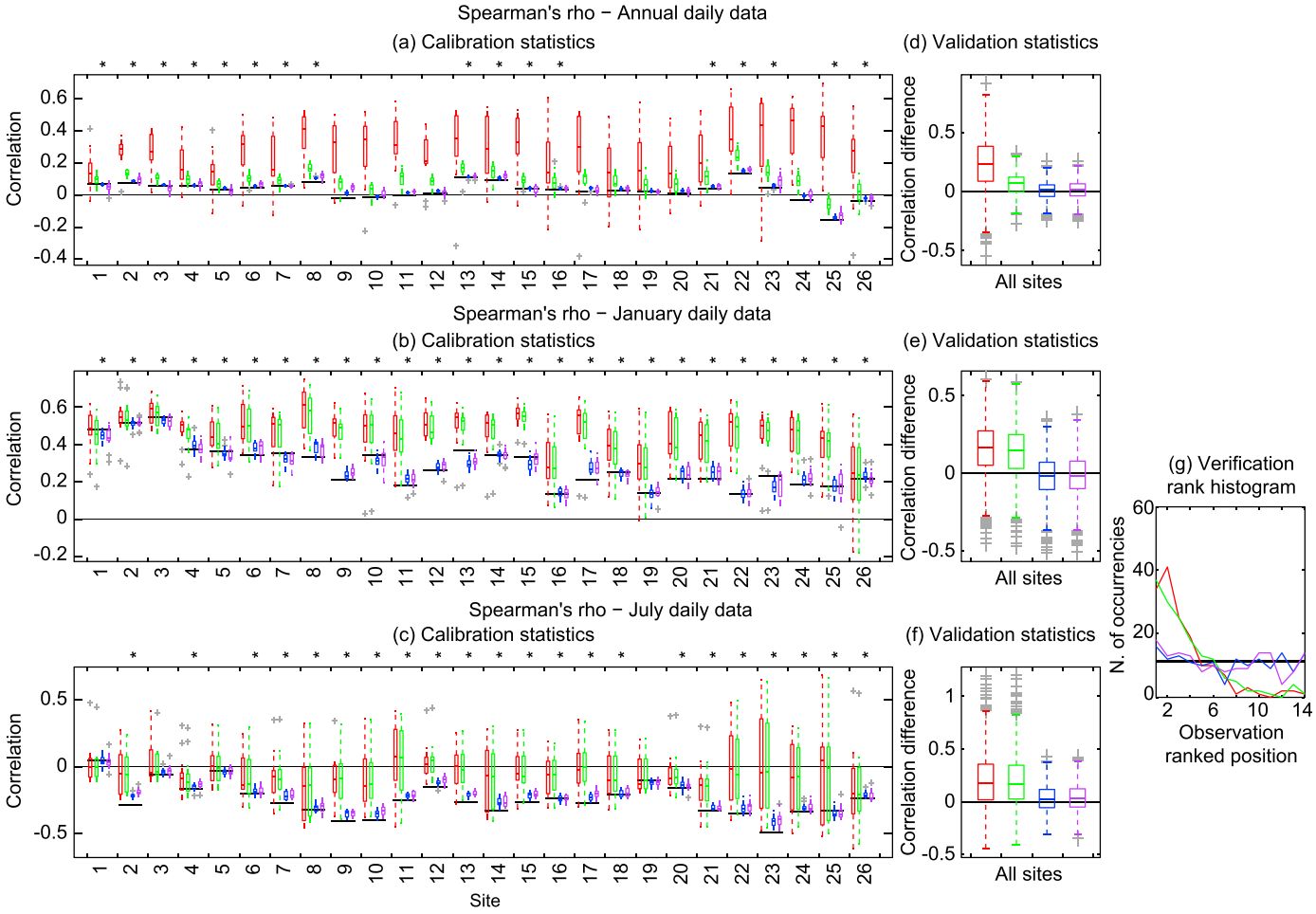

Figure 5. T_{mean}-*Pr* correlation results. (a–c) Boxplots show Spearman's rho values over the full calibration period in observations (black), and DirectSim (red), 1Dqm (green), 2Dqm (blue), and 2Dcopula (violet) scenarios at each site for the ensemble of simulations. Stars on the top of Figures 5a–5c indicate that the correlation in the observations is significant ($p < 0.001$). (d–f) Boxplots show differences in Spearman's rho values between observations and scenarios over the three validation periods at all sites for the ensemble of simulations (1014 values per box). (g) The verification rank histogram based on monthly values. Each colored line represents the frequency distribution of 156 cases (three periods × 26 sites × two months), whereas the horizontal black line represents the ideal distribution.

improve the sharpness of the scenario ensembles in terms of correlation values and the equiprobability of the observational ranks if dry and wet days are mixed (Figures 5d–5g). These improvements are less obvious when dry days are excluded, especially for 2Dqm, which tends to underestimate the correlation coefficients (Figure 6g).

The intervariable dependence was subsequently analyzed with plots showing the empirical nonparametric copula densities of observed and scenario T_{mean} and *Pr* data (e.g., Figures 7, S8, and S9). We used the cell values of these plots to evaluate the degree of similarity of T_{mean}-*Pr* interdependence between observed and scenario data using RMSEs (root-mean-square errors; Figure 8). The main results, supporting those of the intervariable correlation analyses, are the following: (1) The realism of the intervariable dependence improves with the 2-D methods in both the calibration and validation periods, especially for northern sites where the performance of the DirectSim scenarios is worse. (2) For both January and July daily data, the 1Dqm method does not push the modeled empirical copula densities toward the observed ones. (3) For annual daily data, 1Dqm scenarios and observations have more similar empirical copula densities than DirectSim scenarios and observations, but not as similar as those of 2-D scenarios and observations.

Finally, to generalize the results, grid plots were produced showing the ratios between the RMSEs of Figure 8 for each site/simulation pair (Figures 9 and 10 for calibration and validation statistics, respectively). In these plots, ratios greater than one show site/simulation pairs for which the statistical adjustments improve the

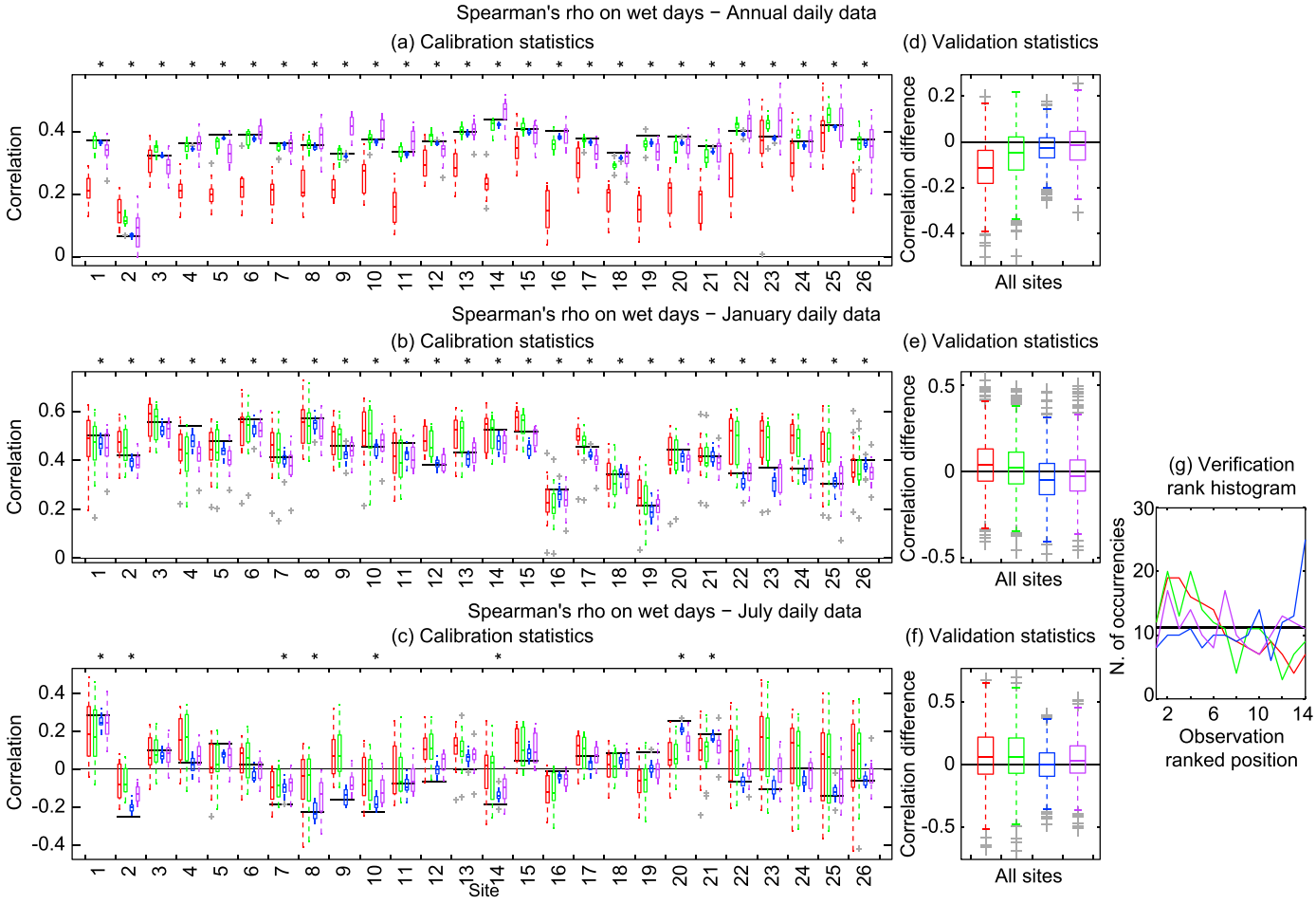

Figure 6. Same as Figure 5, but here dry days were excluded. For scenarios with fewer dry days than observations, dry days were defined as the *n* days with lower *Pr* values where *n* is the number of dry days in the observations.

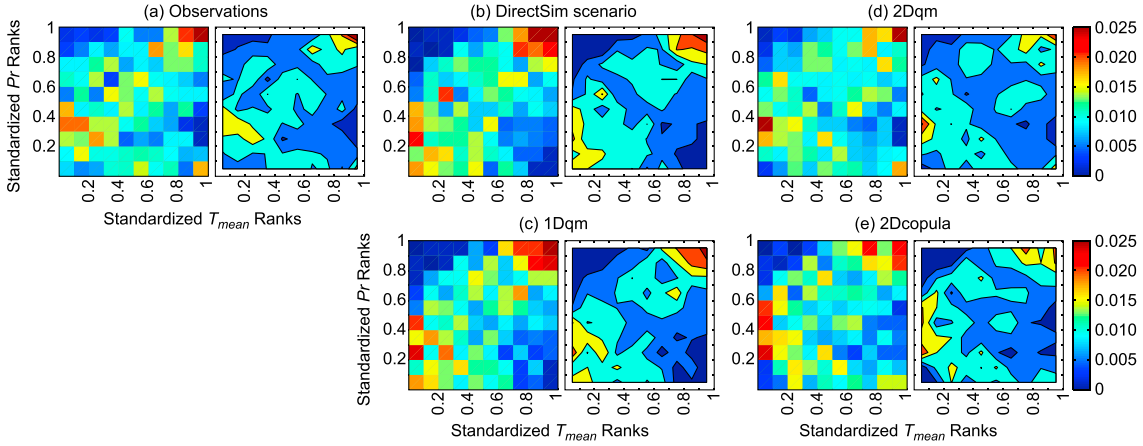

Figure 7. Empirical copula densities of both observed and scenario daily January T_{mean} and *Pr* data over the full calibration period. Copulas for one model (MIROC-ESM) and one site (Resolute) are shown as an example. (a) Observations, (b) DirectSim scenario, (c) 1Dqm, (d) 2Dqm, and (e) 2Dcopula. Two visualizations are visible for each copula: grid plot and contour plot based on the gridded one. Days without rain in each time series are altered by adding a small noise uniformly distributed ranging from 0 mm to the minimum precipitation value. This last step is iterated 100 times, and the average of 100 empirical copulas is plotted.

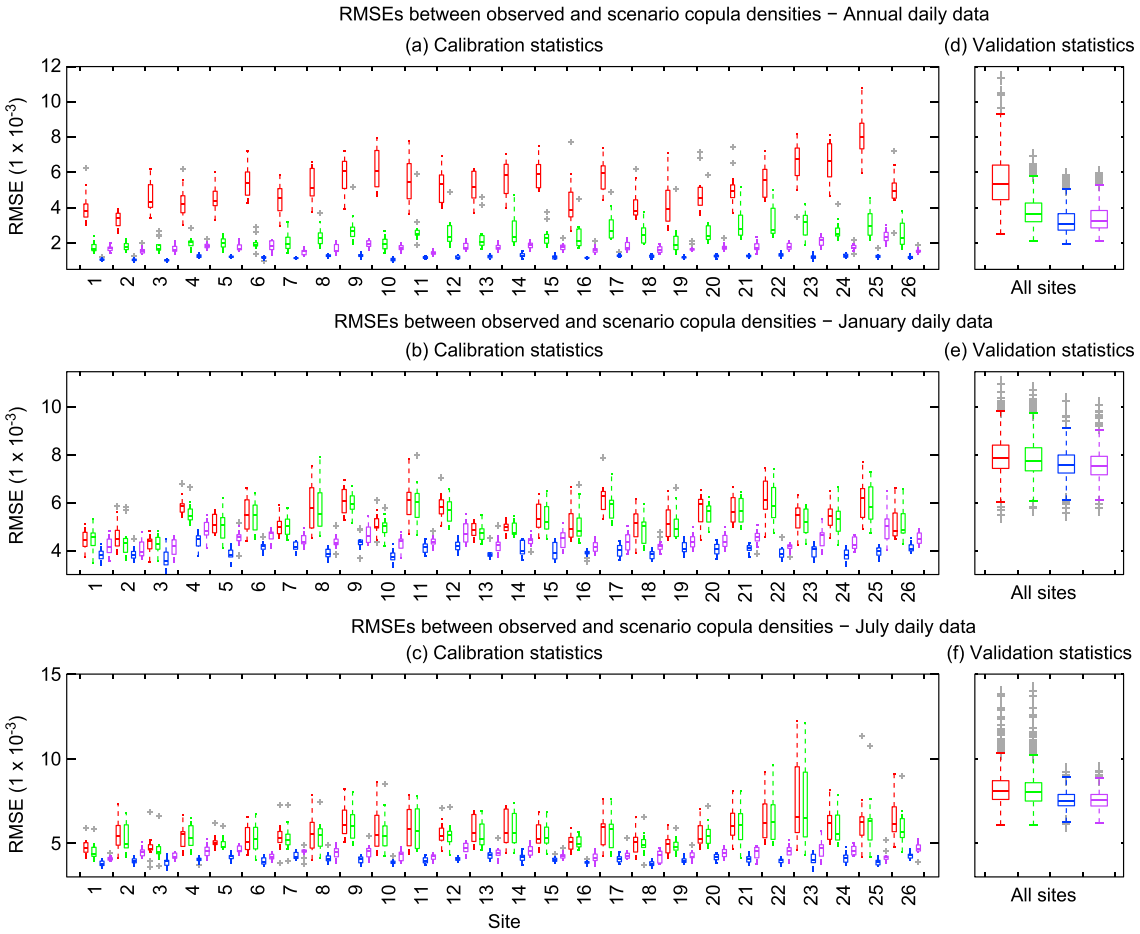

Figure 8. RMSEs between observed and scenario empirical copula densities (see Figure 7 for an example) for (a and d) annual, (b and e) January, and (c and f) July daily data over the full calibration period (Figures 8a–8c) and the three validation periods (Figures 8d–8f). Different colors indicate RMSEs between observations on the one hand and either DirectSim (red), 1Dqm (green), 2Dqm (blue), or 2Dcopula (violet) scenarios on the other.

results relative to DirectSim scenarios (first three columns of plots in Figures 9 and 10) and for which 2Dqm performs better than 2Dcopula (last column of plots in Figures 9 and 10). Once again, we can see that although 2Dqm outperforms all other methods over the full calibration period, 2Dcopula has overall results comparable to those of 2Dqm over the validation periods.

3.3. Impact of Modifications to 2Dqm

Figure 11 shows how the two main modifications applied to the adjustment methods (see section 2.4) improve our scenarios' plausibility. We have compared the linear trends of the mean annual temperatures over the 1981–2035 period of DirectSim and 2Dqm scenarios calibrated over the 1981–2010 period. It is known that quantile mapping can modify climate model simulated trends [*Maurer and Pierce*, 2014]. First, our modified 2Dqm method significantly reduces the alterations introduced by the basic 2Dqm method in the model simulated warming signals (Figure 11a). In our opinion, methods that do not specifically target the trend as the statistical property to be adjusted should leave it unaltered because no change is better than an uncontrolled one. Here we decided to constrain temperature to follow the model simulated trend, but not to do the same for precipitation. The trend preservation for precipitation is more problematic because its trends are more quantile dependent. That is why trends of adjusted precipitation quantiles can be different from the original model trends even after applying a constraint on the average change. To avoid this problem and to improve the preservation of "hydrological sensitivity" (percent change in precipitation per degree of warming), the recently implemented univariate quantile delta mapping approach [*Cannon et al.*, 2015] could be tested in the 2Dqm scheme in future work. Second, our modified 2Dqm method, based on moving

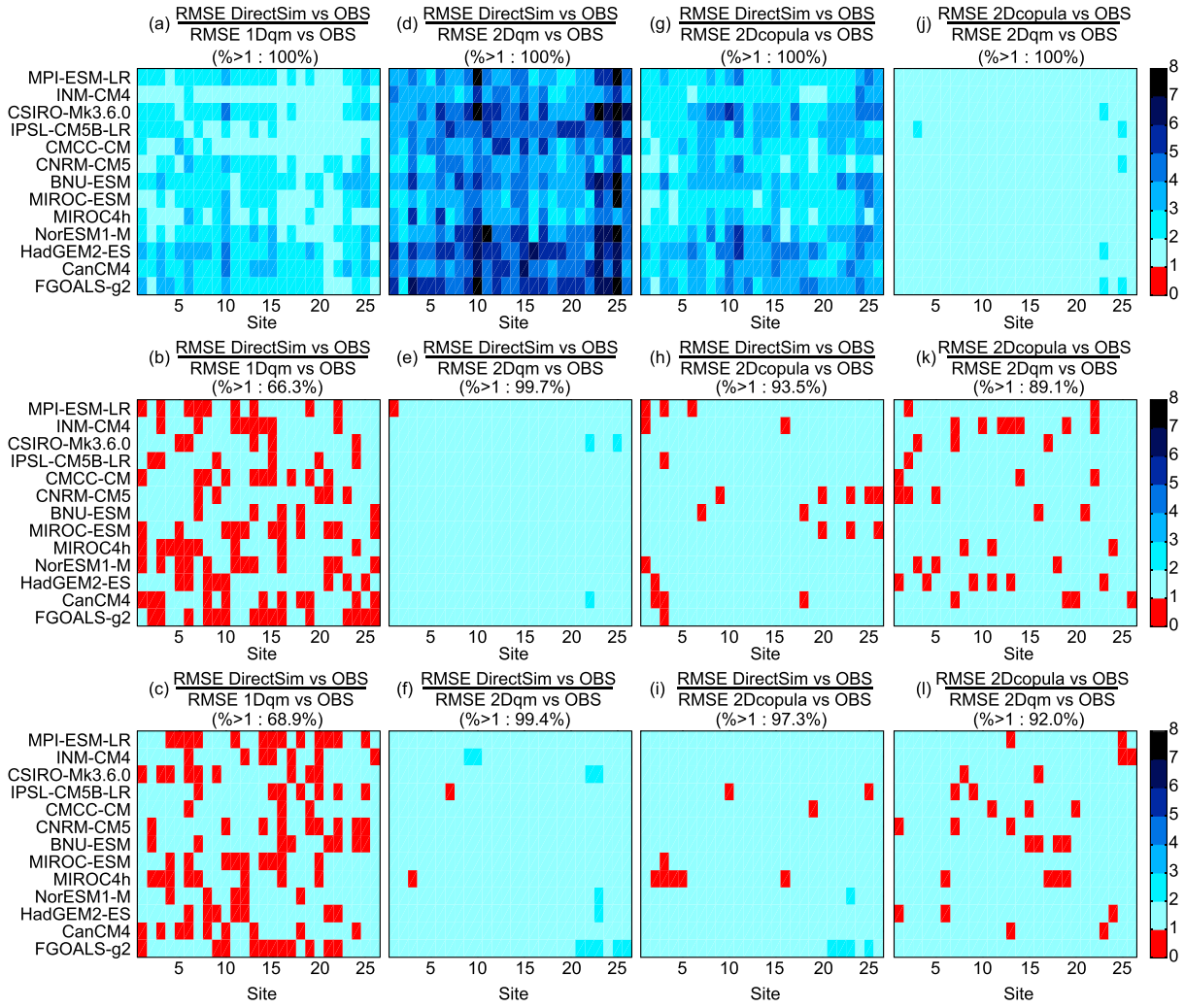

Figure 9. Grids showing ratios between RMSEs of Figures 8a–8c (calibration statistics) for each site/simulation pair. (a, d, g, and j) Results for annual daily data. (b, e, h, and k) Results for daily January data. (c, f, i, and l) Results for daily July data. For each grid plot, the percent of cells with a value greater than one (% > 1) is indicated.

windows to calibrate the transfer functions, avoids artificial jumps in a climate variable's annual cycle at the transition between two successive months compared to a frequently used scheme [e.g., *Lafon et al.*, 2013] calibrating the transfer functions for each month separately (see the spikes in the blue lines of Figure 11b). The potential for jumps in downscaled response through the seasonal cycle has already been highlighted by *Hewitson et al.* [2014].

4. Discussion

The tested 2-D methods, which are upgrades of the methods proposed by *Piani and Haerter* [2012] and *Li et al.* [2014], can satisfactorily adjust individual distributions of T_{mean} and *Pr* time series relative to DirectSim scenarios. In particular, the results of 2Dqm are as good as those of 1Dqm, where T_{mean} and *Pr* are adjusted independently (Figures 4 and S2–S6). Furthermore, the 2-D methods realistically reproduce seasonal variations in the observed T_{mean}-*Pr* interdependence at the selected Canadian Arctic sites, thereby improving the results of the DirectSim and 1Dqm scenarios. As has already been observed elsewhere [*Isaac and Stuart*, 1992; *Rajeevan et al.*, 1998], temperature and precipitation at our sites are in general positively correlated during winter and negatively or not correlated during summer. This is because more snow falls during winter when the temperature is just below 0°C, while rainy days are often cloudier and colder than dry days during the summer. The DirectSim and 1Dqm scenarios are able to reproduce this tendency, but

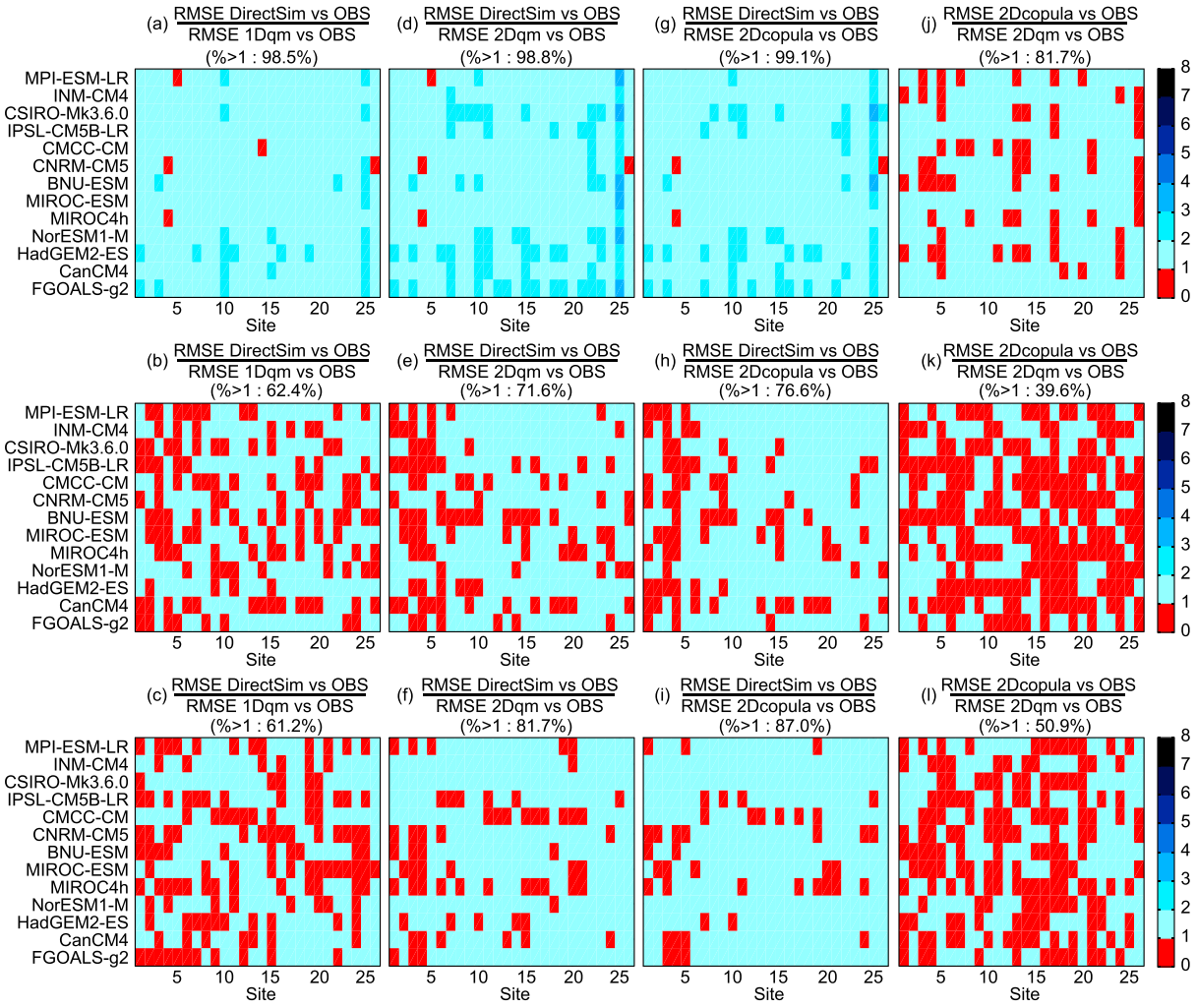

Figure 10. Grids showing ratios between RMSEs of Figures 8d–8f (validation statistics) for each site/simulation pair. Average RMSEs of the three validation periods are used. The setup is the same as that of Figure 9.

the spread among models and the offsets with the observational correlation coefficients are large, especially for northern sites. Conversely, the 2-D methods push the correlation coefficients toward the observed ones and reduce the spread among models in both the calibration and validation periods (Figures 5 and S7). Nevertheless, the adjustments have limitations; for example, when correlations are analyzed for wet days only, the verification rank histogram shows that the 2Dqm ensembles of scenarios tend to underestimate the correlation coefficients over the validation periods (Figure 6g). Because temperature-precipitation interdependence is more complex than can be described by correlation coefficients alone, copulas may be used as a complement [*Cong and Brady*, 2012; *Schölzel and Friederichs*, 2008]. Here we employ empirical copula densities of daily T_{mean} and *Pr* values, and we compare these densities between observed and scenario climatic data (Figures 7, S8, and S9). The results again show that the 2-D scenarios outperform the DirectSim and 1Dqm scenarios in reproducing the observed temperature-precipitation interdependence over the calibration period and improve the scenarios' plausibility over the validation periods (Figures 8–10).

When we compare the performance of the two 2-D methods, all our tests show that 2Dqm clearly outperforms 2Dcopula in reproducing the observational statistics over the full calibration period, but this does not systematically lead to more plausible scenarios over the validation periods (Figures 4–6 and 8–10). This is because 2Dqm is a nonparametric method and is not constrained by the fit between the data and some parametric functions over the calibration period. Instead, over the validation periods, 2Dqm provides some

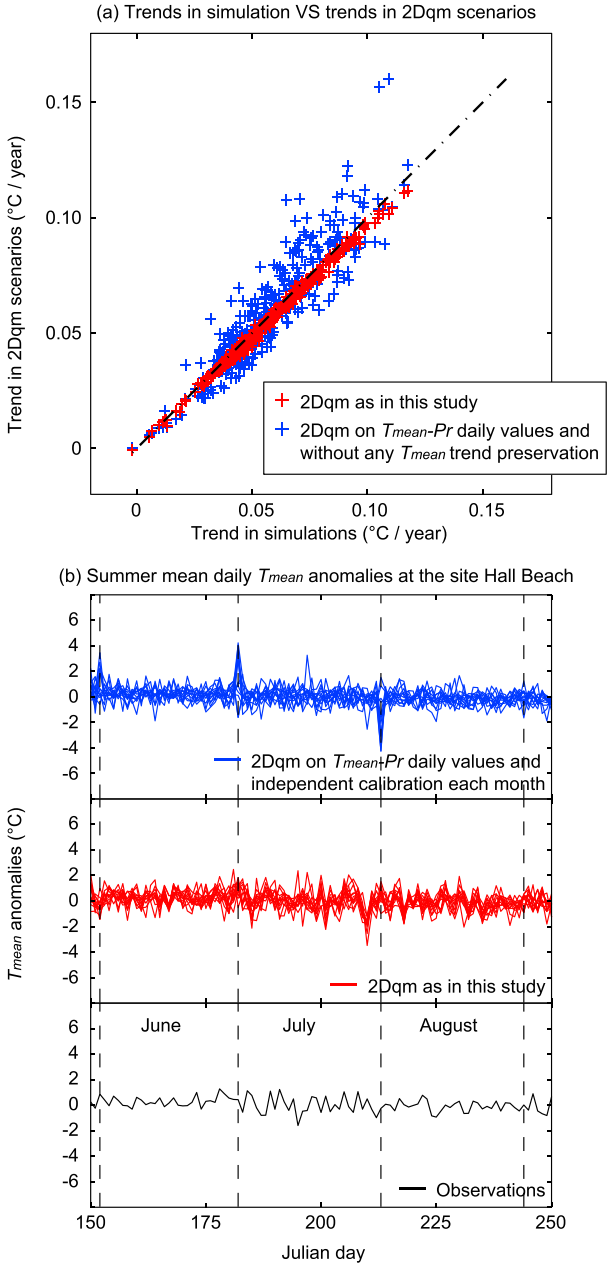

Figure 11. Improvements achieved with the two modifications applied to the adjustment methods in this study. (a) A comparison of mean annual T_{mean} trends over the 1981–2035 period between original simulations (i.e., DirectSim scenarios) and 2Dqm scenarios calibrated over the 1981–2010 period. Trends are slopes of linear regressions fitted to the data. The trend for 338 scenarios is represented (26 sites × 13 simulations). (b) June–August mean daily T_{mean} anomalies relative to the preceding day ($T_{mean_i} - T_{mean_{(i-1)}}$) at the Hall Beach site over the 2001–2010 validation period when 2Dqm scenarios are calibrated over the 1981–2000 period. Values for 13 scenarios are represented.

improvements relative to 2Dcopula for the adjustment of the marginal distributions (Figure 4), but not for the adjustment of the correlation coefficients (Figure 6).

As expected, all adjustment methods produce scenarios which fit the observations over the calibration periods better than over the validation periods (Figures 4–6 and 8–10). Indeed, the scenarios are forced to achieve agreement in some chosen statistical properties over the calibration period and to avoid discontinuities at the junction between the "past" and the "future" segments. Instead, in the validation periods, several causes for the lower agreement of individual scenarios with observations can be considered: (1) the internal climate variability proper to each scenario [*Fischer et al.*, 2014], (2) inhomogeneities in the observational time series [*Mekis*, 2005], (3) possible drift in the simulated offsets over time [*Maraun*, 2012], and (4) in cases like ours, the length of the analyzed period (10 year validation versus 20 or 30 year calibration periods). Thus, over the validation periods we evaluate not only the agreement of the scenarios with the observations, as in other studies [e.g., *Lafon et al.*, 2013; *Li et al.*, 2010; *Stoner et al.*, 2013; *Thrasher et al.*, 2012], but also the sharpness of the scenario ensembles and the equiprobability of the observational ranks among the scenario members.

An important limitation of the tested statistical adjustment methods, which is common to concurrent techniques, is the assumption that the used observational product provides a realistic representation of intervariable dependences. However, there is the possibility that the analyzed statistical properties are misrepresented in the observations. This is especially true in the Arctic, where the station density is poor and crosschecking is more problematic. Furthermore, in the Arctic more than elsewhere, gauge undercatch, regional variation in snowfall density, and trace events can bias the observed precipitation records at the stations [*Mekis*, 2005]. Here to avoid temporal discontinuities, we also use a gridded interpolated data set [*McKenney et al.*, 2011] where precipitation and temperature

are interpolated separately with unknown effect on their interdependence. However, we have to recall that for the moment we are only interested in the performance of the 2-D adjustment methods and that when ready-to-use scenarios will be provided these aspects should be checked comparing different observational products.

5. Conclusion

In this paper we improve and compare two 2-D statistical adjustment methods to produce local climate scenarios with more realistic temperature-precipitation interdependence at Canadian Arctic coastal sites. The improvements consist of modifications previously proposed by univariate statistical adjustment studies [*Hempel et al*., 2013; *Themeßl et al*., 2012; *Thrasher et al*., 2012; *Wood et al*., 2004] (see sections 2.4 and 3.3). Among the proposed methods, 2Dqm outperforms 1Dqm and 2Dcopula over the calibration period (1981–2010). However, better past skills do not necessarily imply better future skills, and indeed our approach to show cross-validation results (see section 2.5) demonstrate that 2Dqm and 2Dcopula perform rather similarly over three validation periods. We did not find any final evidence that would lead us to prefer one method over the other. Future work could test these methods with other climatic variables (e.g., wind, radiation, and humidity), and provide techniques for handling uncertainties in observed data and achieving better characterization of extreme events. Such studies would offer invaluable tools for Arctic users and for the development of appropriate climate change adaptation strategies.

Acknowledgments

The authors are grateful to the modeling centers that contributed the simulations used in this paper, to the Coupled Model Intercomparison Project Phase 5 (CMIP5) of the World Climate Research Programme (WCRP), and to the Earth System Grid Federation for hosting these data (http://pcmdi9.llnl.gov/). The authors also acknowledge the support of Natural Resources Canada, which made the observational data set used in our work available (http://cfs.nrcan.gc.ca/projects/3/4). This study was financially supported by the ArcticNet research program. Finally, the authors wish to thank Ross Brown, Diane Chaumont, Travis Logan, and four anonymous reviewers for their valuable comments on this work.

References

Ben Alaya, M. A., F. Chebana, and T. B. M. J. Ouarda (2014), Probabilistic Gaussian copula regression model for multisite and multivariable downscaling, *J. Clim.*, *27*(9), 3331–3347, doi:10.1175/JCLI-D-13-00333.1.

Brown, R. D. (2000), Northern Hemisphere snow cover variability and change, 1915–97, *J. Clim.*, *13*(13), 2339–2355, doi:10.1175/1520-0442(2000)013<2339:NHSCVA>2.0.CO;2.

Brown, S. J., J. M. Murphy, D. M. H. Sexton, and G. R. Harris (2014), Climate projections of future extreme events accounting for modelling uncertainties and historical simulation biases, *Clim. Dyn.*, *43*(9–10), 2681–2705, doi:10.1007/s00382-014-2080-1.

Cannon, A. J., S. R. Sobie, and T. Q. Murdock (2015), Bias correction of GCM precipitation by quantile mapping: How well do methods preserve changes in quantiles and extremes?, *J. Clim.*, *28*(17), 6938–6959, doi:10.1175/JCLI-D-14-00754.1.

Carroll, M. L., J. R. G. Townshend, C. M. Dimiceli, T. Loboda, and R. A. Sohlberg (2011), Shrinking lakes of the Arctic: Spatial relationships and trajectory of change, *Geophys. Res. Lett.*, *38*, L20406, doi:10.1029/2011GL049427.

Casati, B., A. Yagouti, and D. Chaumont (2013), Regional climate projections of extreme heat events in nine pilot Canadian communities for public health planning, *J. Appl. Meteorol. Climatol.*, *52*(12), 2669–2698, doi:10.1175/JAMC-D-12-0341.1.

Chiew, F. H. S., D. G. C. Kirono, D. M. Kent, A. J. Frost, S. P. Charles, B. Timbal, K. C. Nguyen, and G. Fu (2010), Comparison of runoff modelled using rainfall from different downscaling methods for historical and future climates, *J. Hydrol.*, *387*(1–2), 10–23, doi:10.1016/j.jhydrol.2010.03.025.

Cong, R. G., and M. Brady (2012), The interdependence between rainfall and temperature: Copula analyses, *Sci. World J.*, *2012*, 405675, doi:10.1100/2012/405675.

Dai, A. (2006), Precipitation characteristics in eighteen coupled climate models, *J. Clim.*, *19*(18), 4605–4630, doi:10.1175/JCLI3884.1.

Déqué, M. (2007), Frequency of precipitation and temperature extremes over France in an anthropogenic scenario: Model results and statistical correction according to observed values, *Global Planet. Change*, *57*(1–2), 16–26, doi:10.1016/j.gloplacha.2006.11.030.

Dibike, Y. B., and P. Coulibaly (2005), Hydrologic impact of climate change in the Saguenay watershed: Comparison of downscaling methods and hydrologic models, *J. Hydrol.*, *307*(1–4), 145–163, doi:10.1016/j.jhydrol.2004.10.012.

Fischer, E. M., J. Sedláček, E. Hawkins, and R. Knutti (2014), Models agree on forced response pattern of precipitation and temperature extremes, *Geophys. Res. Lett.*, *41*, 8554–8562, doi:10.1002/2014GL062018.

Fowler, H. J., S. Blenkinsop, and C. Tebaldi (2007), Linking climate change modelling to impacts studies: Recent advances in downscaling techniques for hydrological modelling, *Int. J. Climatol.*, *27*(12), 1547–1578, doi:10.1002/joc.1556.

Genest, C., and A. C. Favre (2007), Everything you always wanted to know about copula modeling but were afraid to ask, *J. Hydrol. Eng.*, *12*(4), 347–368, doi:10.1061/(ASCE)1084-0699(2007)12:4(347).

Germe, A., M. Chevallier, D. Salas y Mélia, E. Sanchez-Gomez, and C. Cassou (2014), Interannual predictability of Arctic sea ice in a global climate model: Regional contrasts and temporal evolution, *Clim. Dyn.*, *43*(9–10), 2519–2538, doi:10.1007/s00382-014-2071-2.

Grenier, P., de Elía R., and D. Chaumont (2015), Chances of short-term cooling estimated from a selection of CMIP5-based climate scenarios during 2006–2035 over Canada, *J. Clim.*, doi:10.1175/JCLI-D-14-00224.1, in press.

Hempel, S., K. Frieler, L. Warszawski, J. Schewe, and F. Piontek (2013), A trend-preserving bias correction—The ISI-MIP approach, *Earth Syst. Dyn.*, *4*(2), 219–236, doi:10.5194/esd-4-219-2013.

Hewitson, B. C., J. Daron, R. G. Crane, M. F. Zermoglio, and C. Jack (2014), Interrogating empirical-statistical downscaling, *Clim. Change*, *122*(4), 539–554, doi:10.1007/s10584-013-1021-z.

Hoffmann, H., and T. Rath (2012), Meteorologically consistent bias correction of climate time series for agricultural models, *Theor. Appl. Climatol.*, *110*(1–2), 129–141, doi:10.1007/s00704-012-0618-x.

Houle, D., A. Bouffard, L. Duchesne, T. Logan, and R. Harvey (2012), Projections of future soil temperature and water content for three southern Quebec forested sites, *J. Clim.*, *25*(21), 7690–7701, doi:10.1175/jcli-d-11-00440.1.

Huang, J., and H. M. van den Dool (1993), Monthly precipitation-temperature relations and temperature prediction over the United States, *J. Clim.*, *6*(6), 1111–1132, doi:10.1175/1520-0442(1993)006<1111:MPTRAT>2.0.CO;2.

Isaac, G. A., and R. A. Stuart (1992), Temperature-precipitation relationships for Canadian stations, *J. Clim.*, *5*(8), 822–830, doi:10.1175/1520-0442(1992)005<0822:TRFCS>2.0.CO;2.

Lafon, T., S. Dadson, G. Buys, and C. Prudhomme (2013), Bias correction of daily precipitation simulated by a regional climate model: A comparison of methods, *Int. J. Climatol.*, *33*(6), 1367–1381, doi:10.1002/joc.3518.
Li, C., E. Sinha, D. E. Horton, N. S. Diffenbaugh, and A. M. Michalak (2014), Joint bias correction of temperature and precipitation in climate model simulations, *J. Geophys. Res. Atmos.*, *119*, 153–162, doi:10.1002/2014JD022514.
Li, H., J. Sheffield, and E. F. Wood (2010), Bias correction of monthly precipitation and temperature fields from Intergovernmental Panel on Climate Change AR4 models using equidistant quantile matching, *J. Geophys. Res.*, *115*, D10101, doi:10.1029/2009JD012882.
Logan, T., I. Charron, D. Chaumont, and D. Houle (2011), Atlas of climate scenarios for Québec forests, *Rep.*, 132 pp., Ouranos and MRNF, Montreal, Canada.
Maraun, D. (2012), Nonstationarities of regional climate model biases in European seasonal mean temperature and precipitation sums, *Geophys. Res. Lett.*, *39*, L06706, doi:10.1029/2012GL051210.
Maraun, D., et al. (2010), Precipitation downscaling under climate change: Recent developments to bridge the gap between dynamical models and the end user, *Rev. Geophys.*, *48*, RG3003, doi:10.1029/2009RG000314.
Maraun, D., M. Widmann, J. M. Gutiérrez, S. Kotlarski, R. E. Chandler, E. Hertig, J. Wibig, R. Huth, and R. A. I. Wilcke (2015), VALUE: A framework to validate downscaling approaches for climate change studies, *Earth's Future*, *3*(1), 2014EF000259, doi:10.1002/2014EF000259.
Maurer, E. P., and D. W. Pierce (2014), Bias correction can modify climate model simulated precipitation changes without adverse effect on the ensemble mean, *Hydrol. Earth Syst. Sci.*, *18*(3), 915–925, doi:10.5194/hess-18-915-2014.
Maurer, E. P., L. Brekke, T. Pruitt, B. Thrasher, J. Long, P. Duffy, M. Dettinger, D. Cayan, and J. Arnold (2014), An enhanced archive facilitating climate impacts and adaptation analysis, *Bull. Am. Meteorol. Soc.*, *95*(7), 1011–1019, doi:10.1175/BAMS-D-13-00126.1.
McKenney, D. W., M. F. Hutchinson, P. Papadopol, K. Lawrence, J. Pedlar, K. Campbell, E. Milewska, R. F. Hopkinson, D. Price, and T. Owen (2011), Customized spatial climate models for North America, *Bull. Am. Meteorol. Soc.*, *92*(12), 1611–1622, doi:10.1175/2011BAMS3132.1.
Mearns, L. O., et al. (2001), Climate scenario development, in *Climate Change 2001. Working Group I: The Scientific Basis. Third Assessment Report of the Intergovernmental Panel on Climate Change*, edited by L. J. Mata and J. Zillman, Cambridge Univ. Press, Cambridge, U. K.
Mekis, É. (2005), Adjustments for trace measurements in Canada, paper presented at Proceedings of the 15th Conference on Applied Climatology, Am. Meteorol. Soc., Savannah, Georgia, 20–24 June.
Mpelasoka, F. S., and F. H. S. Chiew (2009), Influence of rainfall scenario construction methods on runoff projections, *J. Hydrometeorol.*, *10*(5), 1168–1183, doi:10.1175/2009JHM1045.1.
Oldenborgh, G. J. V., F. J. D. Reyes, S. S. Drijfhout, and E. Hawkins (2013), Reliability of regional climate model trends, *Environ. Res. Lett.*, *8*(1), 014055, doi:10.1088/1748-9326/8/1/014055.
Piani, C., and J. O. Haerter (2012), Two dimensional bias correction of temperature and precipitation copulas in climate models, *Geophys. Res. Lett.*, *39*, L20401, doi:10.1029/2012GL053839.
Rajeevan, M., D. S. Pai, and V. Thapliyal (1998), Spatial and temporal relationships between global land surface air temperature anomalies and Indian summer monsoon rainfall, *Meteorol. Atmos. Phys.*, *66*(3–4), 157–171, doi:10.1007/BF01026631.
Räty, O., J. Räisänen, and J. S. Ylhäisi (2014), Evaluation of delta change and bias correction methods for future daily precipitation: Intermodel cross-validation using ENSEMBLES simulations, *Clim. Dyn.*, *42*(9–10), 2287–2303, doi:10.1007/s00382-014-2130-8.
Scherrer, S. C., C. Appenzeller, M. A. Liniger, and C. Schär (2005), European temperature distribution changes in observations and climate change scenarios, *Geophys. Res. Lett.*, *32*, L19705, doi:10.1029/2005GL024108.
Schmidli, J., C. Frei, and P. L. Vidale (2006), Downscaling from GCM precipitation: A benchmark for dynamical and statistical downscaling methods, *Int. J. Climatol.*, *26*(5), 679–689, doi:10.1002/joc.1287.
Schölzel, C., and P. Friederichs (2008), Multivariate non-normally distributed random variables in climate research—Introduction to the copula approach, *Nonlinear Processes Geophys.*, *15*(5), 761–772, doi:10.5194/npg-15-761-2008.
Sklar, A. (1959), *Fonctions De Répartition à n Dimensions Et Leurs Marges*, pp. 229–231, Publications de l'Institut de Statistique de l'Université Paris 8, Paris, France.
Smith, L. C., Y. Sheng, G. M. MacDonald, and L. D. Hinzman (2005), Disappearing Arctic lakes, *Science*, *308*(5727), 1429, doi:10.1126/science.1108142.
Stoner, A. M. K., K. Hayhoe, X. Yang, and D. J. Wuebbles (2013), An asynchronous regional regression model for statistical downscaling of daily climate variables, *Int. J. Climatol.*, *33*(11), 2473–2494, doi:10.1002/joc.3603.
Themeßl, M. J., A. Gobiet, and G. Heinrich (2012), Empirical-statistical downscaling and error correction of regional climate models and its impact on the climate change signal, *Clim. Change*, *112*(2), 449–468, doi:10.1007/s10584-011-0224-4.
Thorne, R. (2011), Uncertainty in the impacts of projected climate change on the hydrology of a subarctic environment: Liard River Basin, *Hydrol. Earth Syst. Sci.*, *15*(5), 1483–1492, doi:10.5194/hess-15-1483-2011.
Thrasher, B., E. P. Maurer, C. McKellar, and P. B. Duffy (2012), Technical Note: Bias correcting climate model simulated daily temperature extremes with quantile mapping, *Hydrol. Earth Syst. Sci.*, *16*(9), 3309–3314, doi:10.5194/hess-16-3309-2012.
Vaughan, D. G., et al. (2013), Observations: Cryosphere, in *Climate Change 2013: The Physical Science Basis, Contribution of Working Group I to the Fifth Assessment Report of the Intergovernmental Panel on Climate Change*, edited by T. F. Stocker et al., Cambridge Univ. Press, Cambridge, U. K., and New York.
Vrac, M., and P. Friederichs (2014), Multivariate—Intervariable, spatial, and temporal—Bias correction, *J. Clim.*, *28*(1), 218–237, doi:10.1175/JCLI-D-14-00059.1.
Wilcke, R. A. I., T. Mendlik, and A. Gobiet (2013), Multi-variable error correction of regional climate models, *Clim. Change*, *120*(4), 871–887, doi:10.1007/s10584-013-0845-x.
Wilks, D. S. (2011), Chapter 7—Statistical forecasting, in *Statistical Methods in the Atmospheric Sciences*, *Int. Geophys. Ser.*, edited by S. W. Daniel, pp. 215–300, Academic Press, New York.
Wood, A. W., L. R. Leung, V. Sridhar, and D. P. Lettenmaier (2004), Hydrologic implications of dynamical and statistical approaches to downscaling climate model outputs, *Clim. Change*, *62*(1–3), 189–216, doi:10.1023/B:CLIM.0000013685.99609.9e.
Ye, H., and J. Cohen (2013), A shorter snowfall season associated with higher air temperatures over northern Eurasia, *Environ. Res. Lett.*, *8*(1), 014052, doi:10.1088/1748-9326/8/1/014052.